Journal of the Physical Society of Japan
Vol. 68, No. 11, November, 1999, pp. 3717-3728

Vacancy-Mediated Phase Separation of Binary Alloy

Toshiya IWAI*

Department of Applied Physics, Graduate School of Engineering, Tohoku University, Aoba-Yama 08, Sendai 980-8579

(Received May 26, 1999)

The most important element process of the phase separation of binary alloys is the vacancy diffusion mechanism. A set of phenomenological dynamical equations for the vacancy-mediated phase separation is formulated from a mean-field free energy and the numerical simulation of the model is performed. From numerical results, vacancies form clusters along phase boundaries between two degenerate stable domains. The width of the vacancy-cluster across the interface grows with the logarithmic function of time. If effects of vacancy-clusters are not dominant, the dynamics is not different from that by the exchange dynamics. If the effects are dominant, the characteristic length proportional to the average domain size grows with the logarithmic function of time. The analytical approach shows that the logarithmic growth of the characteristic length is related to the growth law of the width of the vacancy-cluster.

KEYWORDS: vacancy mechanism, phase separation, conserved order parameter, dynamical scaling

§1. Introduction

Elementary processes of the phase separation of binary alloys are various diffusion processes of atoms. The most important diffusion mechanism in alloys is probably the vacancy mechanism,[1] that is, atoms diffuse simply by exchanging places with vacancies. However, most numerical and theoretical studies of the phase separation have been performed by the exchange mechanism, that is, atoms directly exchange places each other. Kawasaki exchange dynamics[2] is the most typical model of the exchange mechanism. The Cahn-Hilliard(CH) equation[3] is also the phenomenological model of the phase separation by the exchange mechanism. Theoretical and numerical approarches by the exchange mechanism show the dynamical scaling of the scattering function in the late time stage of the phase separation after the rapid quench from a high temperature disordered phase into a low temperature unstable phase.[4-8] The scaling property means the statistically self-similar time evolution of coarsening patterns that is described by the scaling property of the two-body spatial correlation function, $G(r,t) = \mathcal{G}(r/l(t))$, where r, t and $l(t)$ are the distance between two points, time and the characteristic length proportional to the average size of stable domains, respectively. As a result, the Fourier transform of the two-body spatial correlation function, which is called the scattering function $S(k,t)$, also shows the following dynamical scaling property:

$$S(k,t) = l(t)^d \tilde{S}(kl(t)), \tag{1.1}$$

where k, d and $\tilde{S}(x)$ are the wave number, the dimensionality of the system and the scaling function, respectively. The above scaling law is found by scattering experiments[4-6] on the phase separation of binary alloys. As the phase separation proceeds, the characteristic length increases. Theoretical and numerical studies[4-8] show that the growth law of the characteristic length obeys the power law of time and its exponent asymptotically approaches to the value 1/3 in the late time stage when the scaling property is satisfied. Experimental studies[4-6] also show that the exponent value of the power law increases continuously with time and approaches slowly to the value 1/3.

There are not so many studies of the dynamics of the vacancy-mediated phase ordering in a comparison with those of the exchange dynamics. Yaldram and Binder[9,10] carried out Monte Carlo (MC) simulation of the vacancy-mediated phase separation by a three-state spin model. They found that vacancies tended to aggregate at phase boundaries of stable domains. They also found that changing vacancy concentration meant only the change of time scale from the qualitative analysis of the vacancy concentration dependence of the scaling function. MC studies of the phase separation mediated by a single vacancy by Frantzl and Penrose[11,12] demonstrated that the growth law of the characteristic length obeyed the power law of time with its exponent 1/3 in the late time stage for both critical and off-critical quenches. The critical quench means the quench into the low temperature unstable state through the critical point, while the off-critical quench means quenches different from the critical quench. They also numerically studied the coarsening of a cluster of one kind of atom filled in other atoms and found that the cluster diffusion process predominated for the vacancy-mediated phase separation, while the evaporation process predominated for the phase separation by the exchange dynamics. Puri and Sharma[13,14] numerically studied the vacancy-mediated phase dynamics for the critical quench by their mean-field dynamical model. The scaling property of the scattering function and the power growth law

* E-mail: iwai@nlap.apph.tohoku.ac.jp

of the characteristic length with its exponent 1/3 are found from their numerical results.

Vacancies energetically favor to aggregate in the interfacial area between two different stable phases, because the interaction between different two atoms is relatively repulsive in a comparison with that between atoms of the same kind. If the width of the vacancy-cluster across the interface is small, different two atoms are easily exchanged through vacancy-clusters in the interfacial area. However, if the width of the vacancy-cluster becomes large, atoms do not easily exchange through the vacancy-cluster. Consequently, the phase separation dynamics seems to slow down in the latter case. One of our purposes of this study is to investigate the effect of the vacancy-cluster on the phase separation dynamics. We derive a set of phenomenological dynamical equations of the coarse-grained order parameter and the vacancy concentration field from a mean-field free energy and perform the numerical simulation of the dynamical model. We find the following numerical results. (i) The scaling property of the scattering function is satisfied. (ii) The growth law of the characteristic length depends on the coupling parameter of the interaction between the order parameter and the vacancy. If the value of the parameter is small, the characteristic length obeys the power law of time. For the large parameter, the characteristic length obeys the logarithmic law of time. (iii) The width of the vacancy-cluster grows with the logarithmic function of time. (iv) By the analytical approach, the growth law of the characteristic length is shown to be related to the growth law of the width of the vacancy-cluster. In §2, we derive the phenomenological dynamical model from a mean-field free energy. In §3, our method of the numerical simulation is explained. In §4, results of our numerical simulation are shown. In §5, we analytically interprete our numerical results from the phenomenological dynamical model. In §6, we present the summary of our results and discussions.

§2. Model

In this section, a set of phenomenological dynamical equations of the vacancy-mediated phase separation is derived from a mean-field free energy. Although we consider the two-dimensional system in this paper, the discussion below can be easily applied for the three-dimensional system. We explain a mean-field free energy as our starting equation. The system is divided into many square cells with the length of each side Δx. Each cell is labeled by the position vector of the center of the cell scaled by Δx, $\boldsymbol{n}$, so that both components of $\boldsymbol{n}$ take integer. The following simple situation is assumed: each cell includes a macroscopic number of atoms (A-atoms and B-atoms) and vacancies; the volume of an A-atom is the same as that of a B-atom, the volume of a vacancy is defined by that of an atom; the maximum number of atoms included in a cell is assumed to be N_0; the sum of the number of A-atoms in $\boldsymbol{n}$-cell $N_{\mathrm{A},\boldsymbol{n}}$ and that of B-atoms $N_{\mathrm{B},\boldsymbol{n}}$ and that of vacancies $N_{\mathrm{V},\boldsymbol{n}}$ is equal to N_0, that is, a condition $N_{\mathrm{A},\boldsymbol{n}}+N_{\mathrm{B},\boldsymbol{n}}+N_{\mathrm{V},\boldsymbol{n}}=N_0$ is satisfied in any cell. Considering the configurational entropy and interactions among atoms, the mean-field free energy is described as

$$F_{\mathrm{m}} = k_{\mathrm{B}}T\sum_{\boldsymbol{n}}\Big\{N_{\mathrm{A},\boldsymbol{n}}\ln\Big(\frac{N_{\mathrm{A},\boldsymbol{n}}}{N_0}\Big)+N_{\mathrm{B},\boldsymbol{n}}\ln\Big(\frac{N_{\mathrm{B},\boldsymbol{n}}}{N_0}\Big)+N_{\mathrm{V},\boldsymbol{n}}\ln\Big(\frac{N_{\mathrm{V},\boldsymbol{n}}}{N_0}\Big)\Big\}$$
$$-\frac{1}{2}J\sum_{\boldsymbol{n}}\sum_{\boldsymbol{m}\in NN}\Big(N_{\mathrm{A},\boldsymbol{n}}N_{\mathrm{A},\boldsymbol{m}}+N_{\mathrm{B},\boldsymbol{n}}N_{\mathrm{B},\boldsymbol{m}}+\alpha N_{\mathrm{A},\boldsymbol{n}}N_{\mathrm{B},\boldsymbol{m}}+\alpha N_{\mathrm{B},\boldsymbol{n}}N_{\mathrm{A},\boldsymbol{m}}\Big), \tag{2.1}$$

where k_{B}, T and J are the Boltzmann constant, the temperature and the positive coupling constant between atoms of the same kind. αJ is a coupling constant between A and B atoms and we assume $\alpha<1$. In other words, the interaction between atoms of the same kind is attractive, while the interaction between different atoms is weak attractive or repulsive. $\sum_{\boldsymbol{m}\in NN}$ means the sum over nearest neighbor cells of $\boldsymbol{n}$-cell. Due to the restriction $N_{\mathrm{A},\boldsymbol{n}}+N_{\mathrm{B},\boldsymbol{n}}+N_{\mathrm{V},\boldsymbol{n}}=N_0$, $\{N_{\mathrm{A},\boldsymbol{n}}-N_{\mathrm{B},\boldsymbol{n}}\}$ and $\{N_{\mathrm{V},\boldsymbol{n}}\}$ can be chosen as a set of independent variables. Thus, we introduce two order parameters, $\psi_{\boldsymbol{n}}$ and $v_{\boldsymbol{n}}$, by

$$\psi_{\boldsymbol{n}} = (N_{\mathrm{A},\boldsymbol{n}}-N_{\mathrm{B},\boldsymbol{n}})/N_0, \tag{2.2}$$
$$v_{\boldsymbol{n}} = N_{\mathrm{V},\boldsymbol{n}}/N_0 = (N_0-N_{\mathrm{A},\boldsymbol{n}}-N_{\mathrm{B},\boldsymbol{n}})/N_0. \tag{2.3}$$

$\psi_{\boldsymbol{n}}$ represents the order parameter of the phase separation. Positive and negative $\psi_{\boldsymbol{n}}$ correspond to the A-rich and the B-rich phase, respectively. $v_{\boldsymbol{n}}$ is the vacancy concentration. The above mean-field free energy descrived by $\psi_{\boldsymbol{n}}$ and $v_{\boldsymbol{n}}$ is rewritten as

$$F_{\mathrm{m}} = k_{\mathrm{B}}TN_0\sum_{\boldsymbol{n}}\Big\{\frac{1}{2}(1+\psi_{\boldsymbol{n}}-v_{\boldsymbol{n}})\ln\Big(1+\psi_{\boldsymbol{n}}-v_{\boldsymbol{n}}\Big)+\frac{1}{2}(1-\psi_{\boldsymbol{n}}-v_{\boldsymbol{n}})\ln\Big(1-\psi_{\boldsymbol{n}}-v_{\boldsymbol{n}}\Big)+v_{\boldsymbol{n}}\ln v_{\boldsymbol{n}}\Big\}$$
$$-\frac{1}{2}N_0K_0\sum_{\boldsymbol{n}}\sum_{\boldsymbol{m}\in NN}\Big\{\frac{1}{2}(1-\alpha)\psi_{\boldsymbol{n}}\psi_{\boldsymbol{m}}+\frac{1}{2}(1+\alpha)v_{\boldsymbol{n}}v_{\boldsymbol{m}}\Big\}+\text{constant}, \tag{2.4}$$

where $K_0=N_0J$ and linear terms of order parameters are included in the constant term because of conservation laws of order parameters. We choose $\alpha=-1$, because it is a natural assumption that vacancies do not interact each other. This assumption is used in the model formulated by Puri and Sharma.[13,14]

Now, we derive a phenomenological free energy from the above mean-field free energy. If values of order parameters are smaller than unity, the phenomenological free energy like the Ginzburg-Landau free energy is de-

rived by the order parameter expansion of the mean-field free energy. Although both ψ_n and v_n are smaller than unity, the mean-field free energy cannot be expanded by v_n because of the third term in the first summation of eq. (2.4). Thus, we expand the mean-field free energy by only ψ_n and obtain

$$\frac{F}{N_0} = \sum_n \Big[-\frac{1}{2}(\tau_0 - k_B T v_n)\psi_n^2 + \frac{1}{12} k_B T \psi_n^4 + U_0(v_n) \Big] + \frac{1}{4} K_0 N_0 \sum_n \sum_{m \in NN} (\psi_n - \psi_m)^2, \tag{2.5}$$

$$U_0(v) = \frac{1}{2} k_B T[(1-v)\ln(1-v) + v \ln v], \tag{2.6}$$

where $\tau_0 = k_B(T_C - T)$. $T_C = zK_0/k_B$ is the Weiss's mean-field critical temperature[15] and z is the number of nearest neighbors. Terms without U_0 in the first summation in eq. (2.5) represent the local potential of ψ_n with the interaction between ψ_n and v_n. Since the phase separation emerges below the critical temperature, τ_0 is assumed positive. The prefactor of ψ_n^2 in the first term in eq. (2.5) increases as v_n becomes larger. This is qualitatively interpreted by the fact that the mean-field critical temperature decreases as the decrease of the number of neighboring atoms due to replacing atomes with vacancies. U_0 is the the local potential of v_n that is regarded as a restriction of the value of v_n in $(0, 1)$. Thus, we approximate the local potential U_0 by the following simple function for the numerical tractability:

$$U_0(v) = \begin{cases} W_0 v^2 & \text{if } v < 0, \\ W_0(v-1)^2 & \text{if } v > 1, \\ 0 & \text{otherwise,} \end{cases} \tag{2.7}$$

where W_0 is a large positive constant. For covenience, the free energy F is normalized by the quantity $3N_0\tau_0^2/k_B T$ and ψ is normalized by the absolute value of degenerate minimum states of the local potential of ψ_n with $v_n = 0$, $\sqrt{3\tau_0/k_B T}$. Using the normalized order parameter $\tilde{\psi}_n$, the non-dimensional free energy $\tilde{F}$ is described by

$$\tilde{F} = \sum_n \Big\{ -\frac{1}{2}(1 - B v_n)\tilde{\psi}_n^2 + \frac{1}{4}\tilde{\psi}_n^4 + U(v_n) \Big\} + \frac{1}{4} K \sum_n \sum_{m \in NN} (\tilde{\psi}_n - \tilde{\psi}_m)^2, \tag{2.8}$$

where $K = K_0/\tau_0$ and $B = k_B T/\tau_0 = T/(T_C - T)$ is a measure of the degree of the quench depth. $U(v)$ is the same as eq. (2.7) by replacing W_0 by $W = W_0 k_B T/3\tau_0^2$. The phenomenological free energy is derived from the mean-field free energy. We neglect tilde, hereafter.

Next, a dynamical model of the vacancy-mediated phase separation is derived. The phase separation has been usually modeled by partial differential equations. We also describe the dynamical model by terms of partial differential equations. A coarse-grained phenomenological free energy described by the order parameter field $\psi(\boldsymbol{r})$ and the vacancy concentration field $v(\boldsymbol{r})$ is obtained by the continuous limit of spatial variables for the above phenomenological free energy,

$$\mathcal{F} = \int d\boldsymbol{r} \Big\{ \frac{1}{2} K' |\nabla \psi(\boldsymbol{r})|^2 - \frac{1}{2}[1 - B' v(\boldsymbol{r})]\psi(\boldsymbol{r})^2 + \frac{1}{4}\psi(\boldsymbol{r})^4 + U'(v(\boldsymbol{r})) \Big\}, \tag{2.9}$$

where both K', B' and U' are the same as K, B and U in eq. (2.8) except for numerical factors due to the continuous limit of spatial variables, respectively. Although both ψ^2 and ψ^4 terms are also multiplied by numerical factors in general, they are set unity by normalizations of both ψ and the free energy. The explicit expression of parameters in the continuous limit is not important in later discussions. Thus, dashes are neglected, hereafter. A set of dynamical equations for $\psi(\boldsymbol{r}, t)$ and $v(\boldsymbol{r}, t)$ are derived from two principles. One is that the phase separation proceeds to minimize the free energy and the other is the conservation law of both ψ and v. Due to conservation laws of both ψ and v, dynamical equations are described by equation of continuity:

$$\frac{\partial \psi(\boldsymbol{r}, t)}{\partial t} = -\boldsymbol{\nabla} \cdot \boldsymbol{J}_\psi(\boldsymbol{r}, t), \tag{2.10}$$

$$\frac{\partial v(\boldsymbol{r}, t)}{\partial t} = -\boldsymbol{\nabla} \cdot \boldsymbol{J}_v(\boldsymbol{r}, t), \tag{2.11}$$

where $\boldsymbol{J}_\psi$ and $\boldsymbol{J}_v$ are current density vectors at position $\boldsymbol{r}$ and time t for ψ and v, respectively. They are defined by spatial gradients of the local chemical potential. The local chemical potential of the order parameter $\mu_\psi(\boldsymbol{r})$ and that of the vacancy $\mu_v(\boldsymbol{r})$ are defined by functional derivatives of the free energy by order parameters as follows:

$$\boldsymbol{J}_\psi(\boldsymbol{r}, t) = -M(v(\boldsymbol{r}, t))\boldsymbol{\nabla}\mu_\psi(\boldsymbol{r}, t), \tag{2.12}$$

$$\mu_\psi(\boldsymbol{r}, t) = \frac{\delta \mathcal{F}}{\delta \psi(\boldsymbol{r}, t)} = -K\nabla^2\psi - (1 - Bv)\psi + \psi^3, \tag{2.13}$$

$$\boldsymbol{J}_v(\boldsymbol{r}, t) = -M_0 \boldsymbol{\nabla}\mu_v(\boldsymbol{r}, t), \tag{2.14}$$

$$\mu_v(\boldsymbol{r}, t) = \frac{\delta \mathcal{F}}{\delta v(\boldsymbol{r}, t)} = \frac{1}{2} B\psi^2 + \frac{\partial U(v)}{\partial v}, \tag{2.15}$$

where $M(v)$ and M_0 are the mobility of the order parameter and that of the vacancy, respectively. We assume $M(v)$ depends on v, because the current of the order parameter ψ flows only through places where vacancies exist. The detailed expression of $M(v)$ is assumed later. From eqs. (2.10)–(2.15), explicit expressions of dynamical equations of $\psi(\boldsymbol{r})$ and $v(\boldsymbol{r})$ are given by

$$\frac{\partial \psi(\boldsymbol{r}, t)}{\partial t} = -\frac{1}{2}\boldsymbol{\nabla} \cdot \frac{M(v)}{M_0} \boldsymbol{\nabla} \Big\{ \nabla^2\psi + (1 - Bv)\psi - \psi^3 \Big\},$$

$$\frac{\partial v(\boldsymbol{r}, t)}{\partial t} = \frac{1}{2}\nabla^2 \Big\{ \frac{1}{2} B\psi^2 + \frac{\partial U(v)}{\partial v} \Big\}, \tag{2.16}$$

where spatial variables are scaled by $1/\sqrt{K}$ and the temporal variable is scaled by $K/2M_0$. We will use these equations for the interpretation of our numerical results in §5.

§3. Method of Numerical Simulation

In this section, we explain the method of the numerical simulation. In order to compare properties of the va-

cancy mediated phase separation with those of the phase separation described by the exchange mechanism, we also perform the numerical simulation of the CH equation. We explain the difference equation of the CH equation. For the numerical simulation, both spatial and temporal variables are discretized. The two dimensional system is divided into $N \times N$ square cells with $N = 128$. We use the phenomenological free energy F described by eq. (2.8). The dynamical model by discrete variables is derived from the two principles mentioned in the previous section. Therefore, the derivation of the dynamical model for discrete variables essentially implies the discretization of partial differential equations, eq. (2.16). However, we have to perform the discretization carefully because of the vacancy dependence of the mobility. Furthermore, in order to compare the results of our model with those by the CH equation, we have to scale spatial variables by the same normalization factor $1/\sqrt{K}$ that is mensioned below eq. (2.16). Therefore, we replace K in eq. (2.8) by $1/\Delta x^2$.

Now, we derive the dynamical model by discrete variables. Local chemical potentials at $\boldsymbol{n}$-cell are straightforwardly defined by the order parameter derivatives of the free energy eq. (2.8),

$$\mu_{\psi,\boldsymbol{n}}(t) = \frac{\partial F}{\partial \psi_{\boldsymbol{n}}(t)} = -\frac{1}{\Delta x^2}\hat{\Delta}\psi_{\boldsymbol{n}} - (1 - Bv_{\boldsymbol{n}})\psi_{\boldsymbol{n}} + \psi_{\boldsymbol{n}}^3, \tag{3.1}$$

$$\mu_{v,\boldsymbol{n}}(t) = \frac{\partial F}{\partial v_{\boldsymbol{n}}(t)} = \frac{1}{2}B\psi_{\boldsymbol{n}}^2 + \frac{\partial U}{\partial v_{\boldsymbol{n}}}, \tag{3.2}$$

where $\hat{\Delta}$ is the difference operator of the Laplacian in the Euler scheme. If there are no vacancies in both a cell and its nearest neighbor cell, the current of the order parameter between the two cells vanishes. Therefore, the mobility for the current of the order parameter between a cell at $\boldsymbol{n}$ and its nearest neighbor cell at $\boldsymbol{m}$ is assumed proportional to $v_{\boldsymbol{n}} + v_{\boldsymbol{m}}$. The proportional constant is assumed the same as the mobility of the vacancy current M_0. Currents of both the order parameter and the vacancy concentration are assumed to flow along either x axis or y axis. α-component of currents between a cell at $\boldsymbol{n}$ and a cell at $\boldsymbol{n} + \hat{\boldsymbol{\alpha}}$ are described by the following equations:

$$J^{\alpha}_{\psi,\boldsymbol{n}+\hat{\boldsymbol{\alpha}}/2}(t) = -M_0|v_{\boldsymbol{n}+\hat{\boldsymbol{\alpha}}}(t) + v_{\boldsymbol{n}}(t)| \times \frac{\mu_{\psi,\boldsymbol{n}+\hat{\boldsymbol{\alpha}}}(t) - \mu_{\psi,\boldsymbol{n}}(t)}{\Delta x}, \tag{3.3}$$

$$J^{\alpha}_{v,\boldsymbol{n}+\hat{\boldsymbol{\alpha}}/2}(t) = -M_0\frac{\mu_{v,\boldsymbol{n}+\hat{\boldsymbol{\alpha}}}(t) - \mu_{v,\boldsymbol{n}}(t)}{\Delta x}, \tag{3.4}$$

where $\alpha = x, y$ and $\hat{\boldsymbol{\alpha}}$ is the unit vector along α axis. The temporal variable is scaled by $1/2M_0$, so that M_0 in above equations is replaced by $1/2$, hereafter. Dynamical equations of $\psi_{\boldsymbol{n}}$ and $v_{\boldsymbol{n}}$ are described by equation of continuity because of conservation laws of both $\psi_{\boldsymbol{n}}$ and $v_{\boldsymbol{n}}$,

$$\frac{\psi_{\boldsymbol{n}}(t+\Delta t) - \psi_{\boldsymbol{n}}(t)}{\Delta t} = -\sum_{\alpha=x,y}\frac{J^{\alpha}_{\psi,\boldsymbol{n}+\hat{\boldsymbol{\alpha}}/2}(t) - J^{\alpha}_{\psi,\boldsymbol{n}-\hat{\boldsymbol{\alpha}}/2}(t)}{\Delta x}, \tag{3.5}$$

$$\frac{v_{\boldsymbol{n}}(t+\Delta t) - v_{\boldsymbol{n}}(t)}{\Delta t} = -\sum_{\alpha=x,y}\frac{J^{\alpha}_{v,\boldsymbol{n}+\hat{\boldsymbol{\alpha}}/2}(t) - J^{\alpha}_{v,\boldsymbol{n}-\hat{\boldsymbol{\alpha}}/2}(t)}{\Delta x}, \tag{3.6}$$

where Δt is the discretized time unit. Therefore, dynamical equations by discrete variables are defined by eqs. (3.1)–(3.6) with the replacement M_0 with $1/2$. There are four parameters B, W, Δx and Δt in our model . The value of positive parameter $B = T/(T_{\mathrm{C}} - T)$ is choosen 0.1, 0.2 and 0.4 that correspond $T/T_{\mathrm{C}} = 1/11$, $1/6$ and $2/7$, respectively. We choose $W = 10.0$. Since Rogers *et al* [16,17] extensively investigated both spatial and temporal meshes Δx and Δt that give numerically stable solutions of the CH equation, we chose $\Delta x = 1.7$ and $\Delta t = 0.15$ in accordance with their results.

Initial state of the system is a disordered state, so that initial value of $\psi_{\boldsymbol{n}}$ is randomly choosen by the uniform random number in $[-0.05, 0.05]$. Vacancies are assumed to be uniformly distributed initially in the system. Thus, $v_{\boldsymbol{n}}$ takes the same initial value v_0 in each cell. The value of v_0 is choosen 0.001, 0.005, 0.05 and 0.1. Although values 0.05 and 0.1 may be unrealistically large, we perform simulations for these values in order to investigate the v_0 dependence of the dynamics. We numerically solve the above equations by the Runge-Kutta-Gill method untill 10^7 numerical time steps for each set of parameters (B, v_0). To eliminate the dependence on the specific initial state $\{\psi_{\boldsymbol{n}}\}$, eight repetitions of simulations are performed for each set of parameters by use of eight random number sequences and physical quantities are averaged over eight samples. Periodic boundary condition is used.

In order to compare numerical results from the vacancy-mediated phase separation with those by the direct exchange mechanism, we also perform numerical simulation for the phase separation by the CH equation. The original CH equation with the normalized order parameter is described by

$$\frac{\partial \psi(\boldsymbol{r}, t)}{\partial t} = -M_{\mathrm{CH}}\Delta\Big\{K_{\mathrm{CH}}\Delta\psi + \psi - \psi^3\Big\}, \tag{3.7}$$

where M_{CH} and K_{CH} are the mobility and the spatial coupling parameter, respectively. The temporal variable is scaled by $K_{CH}/2M_{\mathrm{CH}}$. Spatial variables are scaled by $1/\sqrt{K_{CH}}$. We can compare spatial properties of the CH dynamics with those of our model by the scaling of spatial variables. The discretized model of the CH equation is as follows:

$$\frac{\psi_{\boldsymbol{n}}(t+\Delta t) - \psi_{\boldsymbol{n}}(t)}{\Delta t} = -\frac{1}{2\Delta x^2}\hat{\Delta}\{\frac{1}{\Delta x^2}\hat{\Delta}\psi_{\boldsymbol{n}} + \psi - \psi_{\boldsymbol{n}}^3\}. \tag{3.8}$$

Since the mobility M_{CH} is not generally the same as M_0 in our model, we have to regard that the time units for two models are not the same. We perform the numerical simulation for the CH dynamics untill 10^6 steps by the same method as our model. Values of parameters, Δx and Δt, and initial configurations of the order parameter are the same as those for the vacancy-mediated phase separation.

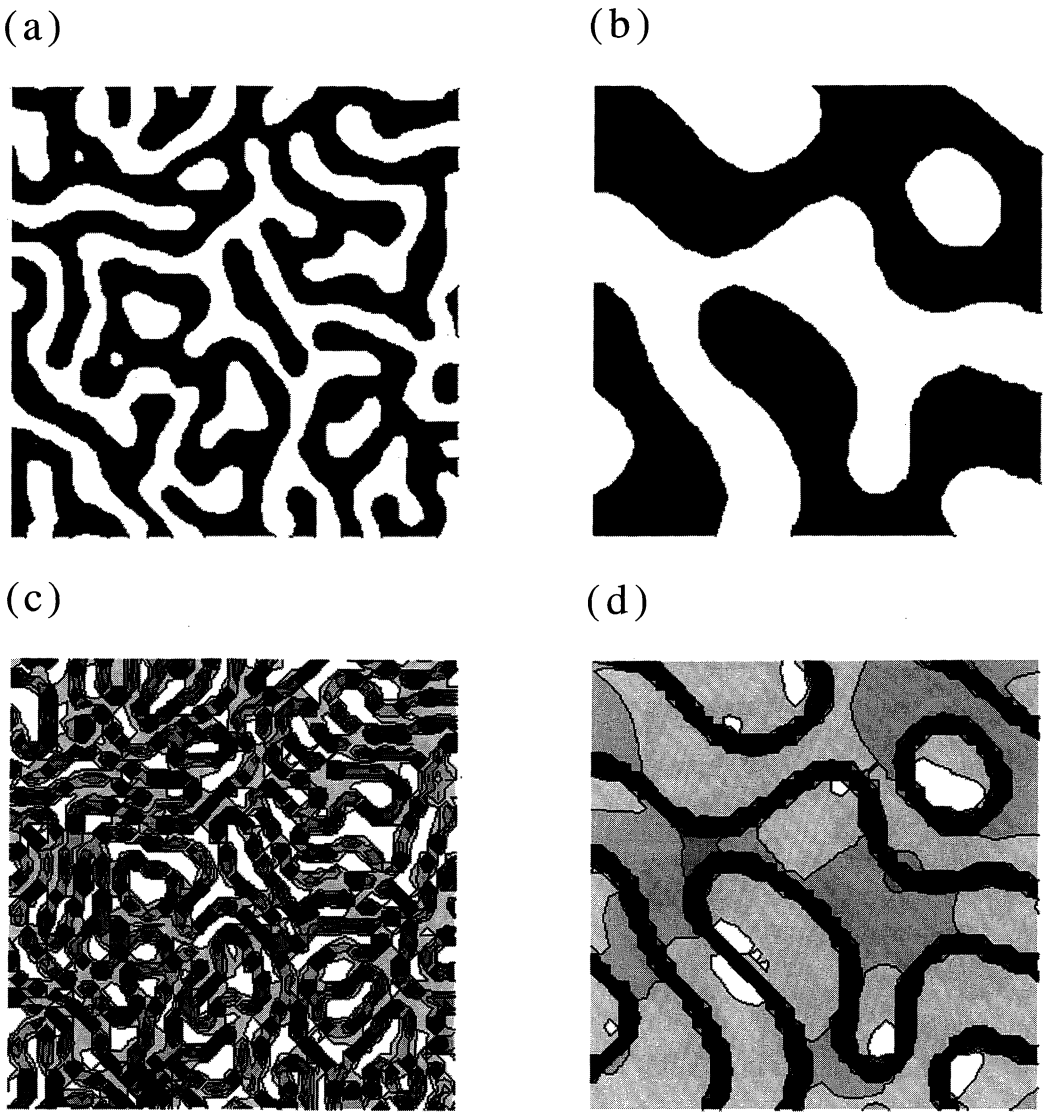

Fig. 1. Contour plots of order parameter and vacancy concentration for $(B, v_0) = (0.1, 0.001)$ on 100×100 cells in the whole system, 128×128 celles. (a) Order parameter at 10^5 steps. (b) Order parameter at 10^6 steps. (c) Vacancy concentration at 10^5 steps. (d) Vacancy density at 10^6 steps.

§4. Results of Numerical Simulation

In this section, we show results of our numerical simulation, the scaling property of the scattering function, the growth law of the charasteristic length and the growth law of both the average width of the interfacial area between two stable domains and the average width of the vacancy-cluster in the interfacial area. Time represents numerical time steps in this section.

4.1 Order parameter and vacancy concentration

Figures 1(a) and 1(b) are contour plots of the order parameter on 100×100 cells in the system for $(B, v_0) = (0.1, 0.001)$ at 10^5 and 10^6 steps, respectively. Black and white areas represent two degenerate stable phases and the boundary between black and white domains is the interface defined by the boundary between two cells where the sign of the order parameter changes. Stable domains of the order parameter grow as time. Figures 1(c) and 1(d) are contour plots of vacancies corresponding to Figs. 1(a) and 1(b), respectively. In these two figures, the color becomes darker as the concentration of vacancies becomes larger. Many domains that are almost stable appear untill 10^4 steps, while vacancies do not form vacancy-clusters before 10^4 steps. Since exchanges of atoms are mediated by vacancies, vacancies are found to aggregate in the interface area as time. As a result, vacancy-clusters are formed along the interface as can be seen in Figs. 1(a) and 1(c) or Figs. 1(b) and 1(d).

Figures 2(a) and 2(b) show topological patterns of interfaces for $(B, v_0) = (0.1, 0.001)$ and $(0.4, 0.001)$, respectively. Fig. 2(c) shows the contour plot of the order parameter for the CH dynamics. Values of the characteristic length in Figs. 2(a)–2(c) take nearly the same value, $l(t) \simeq 2.2$ which is defined later in eq. (4.2). It is difficult to find both the B dependence of topological patterns in Figs. 2(a) and 2(b) and differences between patterns in the vacancy-mediated phase separation and those in the phase separation by the CH equation. However, patterns in Figs. 2(a) and 2(b) seem lougher than those in Fig. 2(c).

Figures 3(a) and 3(b) show profile functions of both

Fig. 2. B dependence of topological patterns of interfaces. Contour plots of order parameter on 100 × 100 cells in the whole system, 128 × 128 celles. (a) $(B, v_0) = (0.1, 0.001)$ at 10^5 steps, (b) $(B, v_0) = (0.4, 0.001)$ at 2×10^5 steps and (c) CH dynamics at 1.6×10^4 steps. The value of the characteristic length, l, in all figures is nearly equal to 2.2. l is defined in eq. (4.2).

the order parameter and the vacancy at 10^7 steps for $v_0 = 0.001$ and 0.1, respectively. In these figures solid lines represent profile functions of the order parameter,

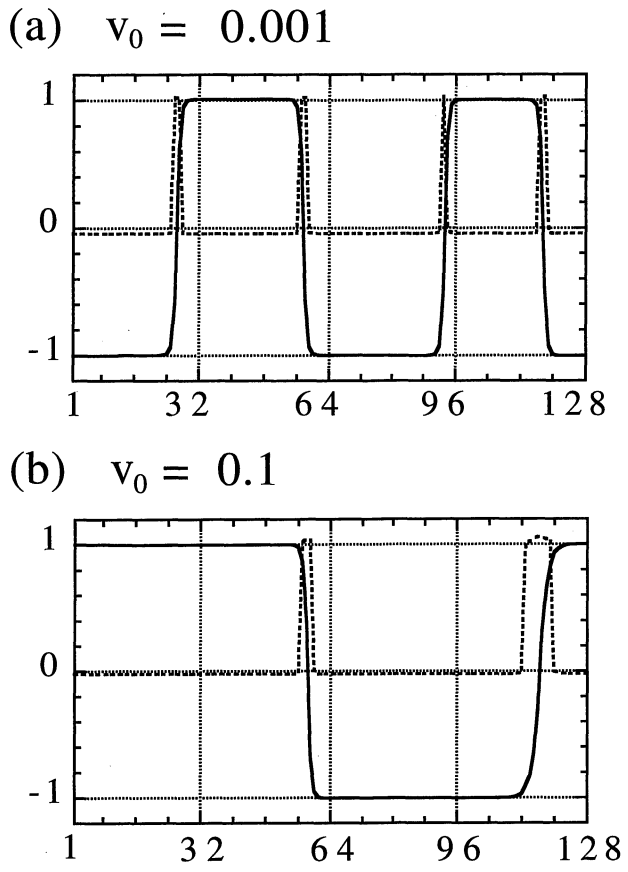

Fig. 3. Profile functions of order parameter and vacancy concentration for $B = 0.1$ at 10^7 steps for $v_0 = 0.001$ (a) and $v_0 = 0.1$ (b). Solid lines represent order parameter profile. Dotted lines represent vacancy profile.

while dotted lines represent those of the vacancy concentration. The vacancy concentration in stable domains is much smaller than that in the interfacial area. that is. the vacancy-cluster is formed along the interface. In the interfacial area, the spatial variance of the vacancy concentration across the interface is sharper than that of the order parameter. The width of the interfacial area of the order parameter seems larger than that of the vacancy-cluster. As v_0 becomes larger, the width of the vacancy-cluster becomes wider. The width of the interfacial area also becomes larger with the increase of the width of the vacancy-cluster. The time dependence of both the width of the vacancy-cluster and that of the interfacial area is discussed later in detail.

4.2 Scaling property of scattering function

We investigate the following scaling property of the scattering function:

$$\langle S(k,t) \rangle = l(t)^2 \tilde{S}(kl(t)), \tag{4.1}$$

where angle brackets mean the average over eight samples and $S(k,t)$ is the angular averaged scattering function. The characteristic length $l(t)$ is usually defined by the inverse of the first moment of the scattering function described as

$$l(t) = \left\langle \frac{\sum_k S(k,t)}{\sum_k kS(k,t)} \right\rangle. \tag{4.2}$$

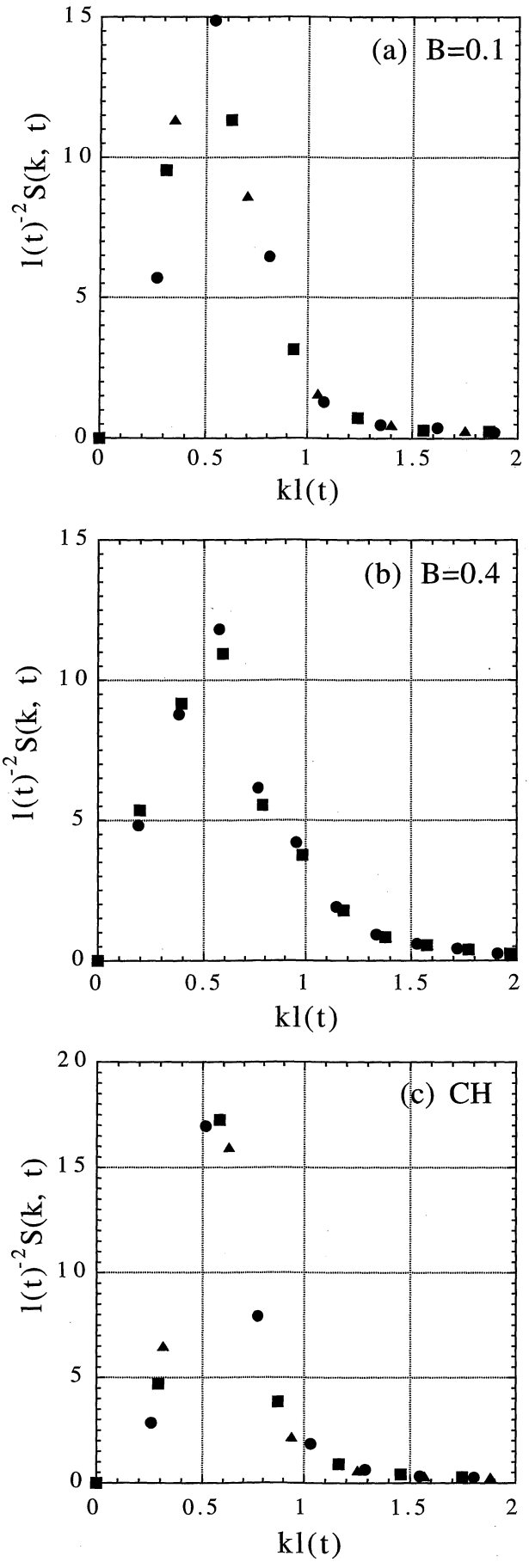

Fig. 4. Scaling plots for scattering functions, $l(t)^{-2}S(k,t)$ vs $kl(t)$ at 4×10^6(circle), 7×10^6(square) and 10^7(triangle) steps for $(B, v_0) = (0.1, 0.001)$ (a) and $(B, v_0) = (0.4, 0.001)$ (b). (c) Scaling plot at 4×10^5(circle), 6×10^5(square) and 8×10^5(triangle) steps for the CH dynamics.

Figures 4(a) and 4(b) show scaling plots, $l(t)^{-2}S(kl(t),t)$ versus $kl(t)$, for $B = 0.1$ and $B = 0.4$, respectively. In each figure, data at 4×10^6, 7×10^6 and 10^7 steps are plotted. Scaling plots of these three different time steps are fitted on a single curve. Therefore, the scaling property is satisfied in the late time region of the vacancy-mediated phase separation. This result is consistent with studies by Puri and Sharma.[13,14] On the other hand, the scaling property is known to be satisfied in the late time region of the phase separation described by the exchange dynamics.[4-8] We also show scaling plots of the phase separation by the CH equation in Fig. 4(c) where data at 4×10^5, 6×10^5 and 8×10^5 steps are plotted. Since scaling plots in this figure are fitted on a single curve, the scaling property for the CH dynamics is also satisfied. From Figs. 4(a) and 4(b), the scaling function for $B = 0.1$ is diffrent from that for $B = 0.4$. The scaling function for $B = 0.4$ in large k region is larger than that for $B = 0.1$ and the peak height for $B = 0.1$ is higher than that for $B = 0.4$. Therefore, as B becomes larger, there seem to be much more small scale structures around the phase boundary. Furthermore, the scaling function for the CH dynamics in Fig. 4(c) is also different from those in Figs. 4(a) and 4(b). The peak height in the case of the CH dynamics is higher than those in the case of the vacancy-mediated phase separation. The width of the peak in the CH case is narrower than those in the case of the vacancy-mediated phase separation. Subtle topological differences of coasening patterns in Figs. 2(a)–2(c) seem to indicate the cause of differences in scaling functions. These results suggests that interfaces for vacancy-mediated dynamics easily become rough. This is consistent with the fact that vacancies around interfaces reduce the interfacial energy.

4.3 Growth law of characteristic length

The characteristic length becomes larger as the phase separation proceeds. Figures 5(a) and 5(b) illustrate the time dependence of the characteristic length for $B = 0.1$ and $B = 0.4$, respectively. There are qualitative differences between growth laws of the characteristic length for $B = 0.1$ and $B = 0.4$. Thus, in the case of $B = 0.1$, the logarithmic function of $l(t)$ is plotted versus the logarithmic function of time in Fig. 5(a). On the other hand, in the case of $B = 0.4$, $l(t)$ is plotted versus logarithmic function of time in Fig. 5(b). In these figures, solid line, dashed line, dotted line and dashed-and-dotted line represent $l(t)$ for $v_0 = 0.001$, 0.005, 0.05 and 0.1, respectively. The growth rate before 10^5 steps depends on the value of v_0 as in both Figs. 5(a) and 5(b), while that after 10^5 steps seems qualitatively independent of the value of v_0.

For $B = 0.1$, the characteristic length after 10^6 steps satisfies the power law of time, $l(t) \propto t^a$. The time region where the power law is found in Fig. 5(a) is wider as v_0 becomes larger. The exponent of power law is numerically calculated by the least square method between 10^6 and 10^7 steps that is written on Table I. There are 900 data points between 10^6 and 10^7 steps. Errors of the exponent δa are evaluated by the mean square deviation of data, D, from the numerically estimated power

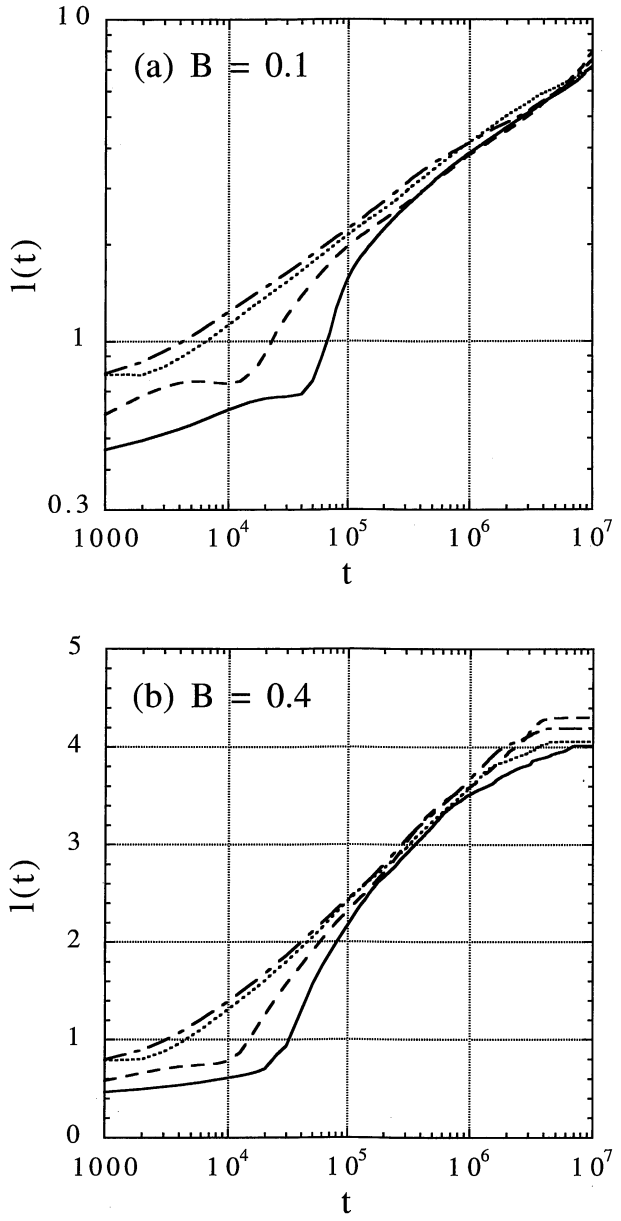

Fig. 5. Time dependence of $l(t)$. (a) Plots of logarithmic function of $l(t)$ vs logarithmic function of t for $B = 0.1$. (b) Plots of $l(t)$ vs logarithmic function of t for $B = 0.4$. Solid lines, dashed lines, dotted lines and dashed-and-dotted lines are $l(t)$ for $v_0 = 0.001$, 0.005, 005 and 0.1, respectivey.

law, that is, $\delta a = \pm D/(\ln 10^7 - \ln 10^6)$. The error is also written on Table I. In the case of the CH dynamics, the characteristic length is found to obey the power law of time. Its exponent calculated between 10^5 and 10^6 steps is also written on Table I. Moreover, another characteristic length $r(t)$ defined below is calculated for both the vacancy-mediated phase separation and the phase separation described by the CH equation:

$$r(t) = \langle 2N^2/l_i(t)\rangle, \tag{4.3}$$

$$l_i(t) = \sum_{\boldsymbol{n}}[\theta(-\psi_{\boldsymbol{n}}(t)\psi_{\boldsymbol{n}+\hat{\boldsymbol{x}}}(t)) + \theta(-\psi_{\boldsymbol{n}}(t)\psi_{\boldsymbol{n}+\hat{\boldsymbol{y}}}(t))], \tag{4.4}$$

where $\theta(x)$ is a step function. $l_i(t)$ is the number of bonds between nearest neighbor cells where the sign of the order parameter changes. This quantity is roughly equal to the total interfacial length. $2N^2$ is the total number of bonds. Thus, $r(t)$ approximately represents the average domain size at time t. The time dependence of $r(t)$ is almost the same as that of $l(t)$ in Figs. 5(a) and 5(b). Numerically evaluated exponent values for $r(t)$ during the same period as that for $l(t)$ are also written on Table I. The exponent in the CH case takes the value 0.331 consistent with the many experimental and theoretical studies.[4-6] In the case of vacancy-mediated dynamics, exponent values except for one case are less than 1/3. Since exponent values evaluated between 10^5 and 10^7 steps are less than those in Table I for each parameter set, exponent values seem to become larger slowly with time. Therefore, exponent values may approach to the value 1/3 after 10^7 steps. Therefore, these results show that for small B the growth law of the characteristic length is not different from that for the exchange dynamics qualitatively.

Table I. Exponent a of power law of both $l(t)$ and $r(t)$ between 10^6 and 10^7 steps for vacancy-mediated phase separation. Exponent for CH dynamics are also calculated between 10^5 and 10^6 steps. δa is the error evaluated from mean square deviation of data points from the power law.

B	v_0	$a \pm \delta a$ for $l(t)$	$a \pm \delta a$ for $r(t)$
0.1	0.1	0.242 ± 0.011	0.270 ± 0.007
0.1	0.05	0.237 ± 0.009	0.262 ± 0.011
0.1	0.005	0.301 ± 0.013	0.339 ± 0.014
0.1	0.001	0.267 ± 0.005	0.315 ± 0.007
CH	—	0.299 ± 0.009	0.331 ± 0.007

For $B = 0.4$, the characteristic length after 10^5 steps is approximately fitted on a straight line proportional to the logarithmic function of time as can be seen in Fig. 5(b), although the growth law of $l(t)$ for $v_0 = 0.1$ seems to satisfy power law between 10^3 and 10^5 steps. Furthermore, the growth rate slows down after about 3×10^6 steps. Thus, the dynamics for large B is found slower than that for small B. If most of vacancies aggregate in vacancy-clusters, atoms do not easily exchange through vacancies. This seems to be the reason of slowing down of the dynamics. We give analytical interpretations about the B dependence of the growth law of the characteristic length in §5.

4.4 Interfacial area and vacancy-cluster

We investigate the dynamics for both the average width of the interfacial area between two stable states and that of the vacancy-cluster in the interfacial area. The following quantities are numerically calculated as a function of time:

$$A(t) = \sum_{\boldsymbol{n}} \theta(0.8 - \psi_{\boldsymbol{n}}(t)^2), \tag{4.5}$$

$$A_v(t) = \sum_{\boldsymbol{n}} \theta(v_{\boldsymbol{n}}(t) - 0.2)\theta(0.8 - \psi_{\boldsymbol{n}}(t)^2). \tag{4.6}$$

$A(t)$ represents the total area of phase boundaries of the order parameter called the interfacial area in this paper. $A_v(t)$ represents the total area of vacancy-clusters in the interfacial area. The average width of the interfacial area

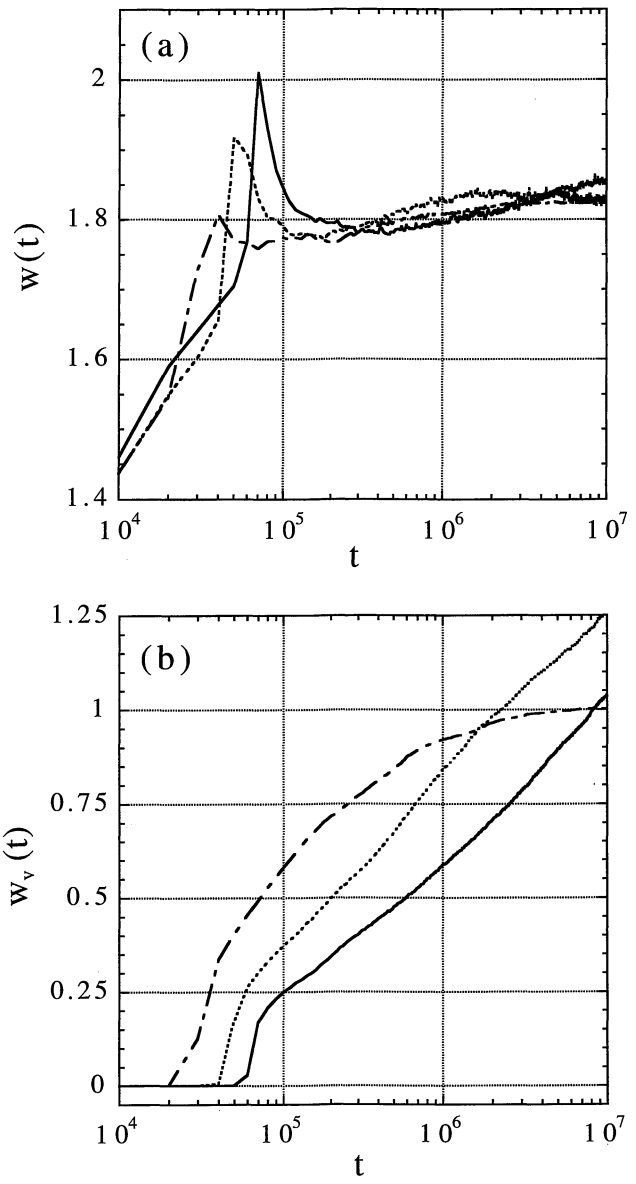

Fig. 6. Time dependence of widths of both interfacial area and vacancy-cluster for $v_0 = 0.001$. Solid lines, dashed lines and dashed-and-dotted lines represent cases for $B = 0.1$, 0.2 and 0.4, respectively. (a) Width of interfacial area vs logarithmic function of time. (b) Width of vacancy-cluster vs logarithmic function of time.

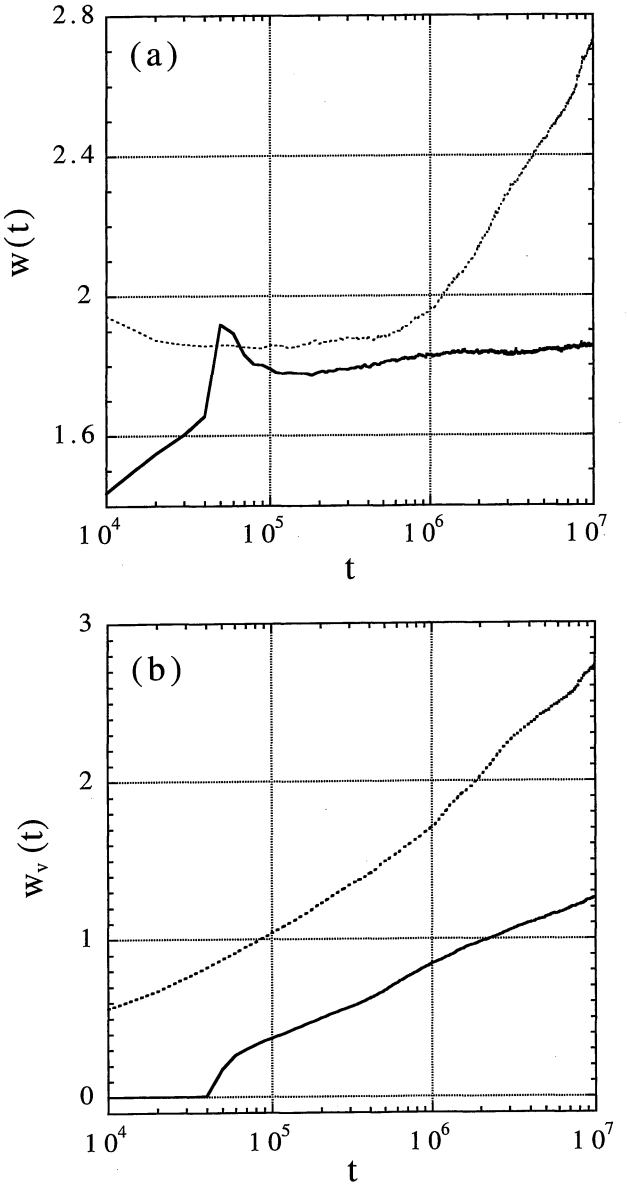

Fig. 7. Time dependence of widths of both interfacial area and vacancy-cluster for $B = 0.2$. Solid lines and dotted lines represent cases for $v_0 = 0.001$ and 0.1, respectively. (a) Width of interfacial area vs logarithmic function of time. (b) Width of vacancy-cluster vs logarithmic function of time.

$w(t)$ and that of vacancy-cluster $w_v(t)$ are defined by

$$w(t) = \langle A(t)/l_i(t) \rangle, \tag{4.7}$$

$$w_v(t) = \langle A_v(t)/l_i(t) \rangle, \tag{4.8}$$

where $l_i(t)$ defined by eq. (4.4) is the total interfacial length.

Figires 6(a) and 6(b) show the time dependence of w and w_v for various values of B, respectively. The value of v_0 in these figures is equal to 0.001. w rises dramatically to a peak before 10^5 steps and remains almost the constant value 1.8 after 10^5 steps, while w obtained from numerical simulation by the CH equation remains a constant value 1.15 after 10^4 steps. The vacancy-cluster with a finite width excludes the order parameter from the interfacial area. Consequently, the value of w for the vacancy dynamics is larger than that for the exchange dynamics. On the other hand, w_v is nearly equal to zero in the early time region before $2 \sim 5 \times 10^4$ steps, increses rapidly for a while and grows steadily after about 10^5 steps as in Fig. 6(b). The growth law of w_v for $B = 0.1$ and 0.2 satisfies the logarithmic function of time after 10^5 steps, while w_v for $B = 0.4$ illustrates slower growth than the logarithmic function of time. The logarithmic growth law of w_v seems to be related with the growth law of the characteristsic length in Fig. 5(b). This fact is investigated in §5. The value of w_v for $B = 0.2$ is larger than that for $B = 0.1$. The value of w_v for $B = 0.4$ before 10^6 steps is the largest among them, although w_v for $B = 0.4$ slows down after 10^6 steps. We give a conjecture about these features of w_v as follows. Since currents of vacancies are proportional to B as in eqs. (2.14) and (2.15), vacancies are easier to move as B becomes larger.

Consequently, the growth of w_v becomes larger with B before 10^6 steps in Fig. 6(b). If most of vacancies aggregate in vacancy-clusters, the growth of the width of the vacancy-cluster slows down because of the conservation law of the vacancy. We suppose that the slowing down of w_v for $B = 0.4$ in Fig. 6(b) shows such a situation.

The growth rate of w for large v_0 is different from that for small v_0. w for both $v_0 = 0.1$ and 0.001 are shown in Fig. 7(a) for $B = 0.2$, while w_v corresponding to Fig. 7(a) are shown in Fig. 7(b). w for $v_0 = 0.1$ steadily increases as time after about 10^6 steps, while w for $v_0 = 0.01$ remains almost constant after 10^5 steps. On the other hand, the growth law of w_v for both $v_0 = 0.001$ and 0.1 seems to satisfy the logarithmic growth law of time, althoght the value of w_v for $v_0 = 0.1$ is about two times larger than that for $v_0 = 0.001$. Since the value of w_v for $v_0 = 0.1$ is comparable with the value of w for $v_0 = 0.1$ at about 10^6 steps, it is reasonable that w begins to grow accompanied with the growth of w_v after 10^6 steps. Thus, w for $v_0 = 0.001$ may also begin to grow after 10^7 steps.

§5. Analytical Interpretation of Numerical Results

In this section, we qualitatively interpret results of our numerical simulation for small v_0 by use of the dynamical model with contiuous variables, eq. (2.16). The vacancy-mediated phase separation for small v_0 seems to be divided into the following three stages as found in Figs. 6(a) and 6(b): (i) many stable domains apear, while vacancies do not order in interfacial area before about $2 \sim 5 \times 10^4$ steps in Figs. 6(a) and 6(b), (ii) vacancies aggregate in the interfacial area and form vacancy-clusters along the interface between $2 \sim 5 \times 10^4$ and 10^5 steps in Fig. 6(b), (iii) the growth rate of the width of the vacancy-cluster satisfies the logarithmic law of time for $B = 0.1$ and 0.2 after 10^5 steps in Fig. 6(b). We call these three time stages the first, second and third stages, respectively.

Now, we investigate the growth law of both the characteristic length and the width of the vacancy-cluster in the second and third stages for the case of small v_0. Although the width of the interfacial area in the second stage varies with time, the deviation of the width from the constant value 1.8 is, at most, 0.2 as in Fig. 6(a). In the third stage, the width of the interfacial area remains constant value 1.8. Thus, the width of the interfacial area is assumed independent of time for small v_0 in both second and third stages. The initial state in the seond stage is assumed as follows for the analytical tractability: stable domains are separated far away, so that direct interactions between them except for the conservation law of the order parameter can be ignored; although the shape of the typical stable domain is not the circle, we consider the spherical domain with a radius R. Analytical approaches by use of these assumptions have been succeeded for the study of the phase separation by both the famous Lifshtz-Slyozov theory[18] and the statistical theory by Kawasaki *et al.*[19,20] Thus, we assume the order parameter field of a spherical domain as

$$\psi(\boldsymbol{r}, t) = \psi_0 \tanh([R(t) - r]/w), \tag{5.1}$$

where ψ_0 and r are the amplitude of the order parameter and the radial variable, respectively. Time independent constants w and ψ_0 are defined later. We assume $R \gg w > w_v$ during both second and third stage and $w \gg w_v$ at the initial state in the second stage. Since the spatial variance of the vacancy-cluster across the interface is much sharper than that of the order parameter as in Figs. 3(a) and 3(b), the vacancy field $v(r,t)$ is assumed to take unity in $|r - R| < w_v/2$ and sufficiently small value δ in $|r - R| \geq w_v/2$. Thus, we assume the functional form of $v(r,t)$ as

$$v(r,t) = \begin{cases} 1 & \text{if } |r - R(t)| < w_v(t)/2, \\ \delta & \text{if } |r - R(t)| > w_v(t)/2, \end{cases} \tag{5.2}$$

The time dependence of δ is ignored, because δ is recognized to be sufficiently small. Equation (2.16) is reproduced for convenience as our starting equations:

$$\frac{\partial \psi(\boldsymbol{r}, t)}{\partial t} = -\boldsymbol{\nabla} v \cdot \boldsymbol{\nabla}\{f(\psi)\}, \tag{5.3}$$

$$f(\psi(\boldsymbol{r}, t)) = \frac{1}{2}\nabla^2\psi + (1 - Bv)\psi - \psi^3, \tag{5.4}$$

$$\frac{\partial v(\boldsymbol{r}, t)}{\partial t} = \nabla^2\{\frac{1}{2}B\psi^2\}, \tag{5.5}$$

where the mobility of the current of ψ, $M(v)$ in eq. (2.16), is assumed $M_0 v$, because of the same reason of our numerical model, that is, the current of the order parameter vanishes at the place where v vanishes. The time dependene of both R and w_v is obtained by the analysis of eqs. (5.1)–(5.5). ψ defined by eq. (5.1) with $\psi_0 = w^{-1} = \sqrt{1 - B\delta}$ is the approximate solution of eq. (5.3) for $|r - R| \gg w$, because $f(\psi) = -\frac{1}{2rw}\psi_0 \mathrm{sech}^2([r - R]/w) \simeq 0$ at $|r - R| \gg w$.

First, we investigate the growth law of w_v from eq. (5.5). w_v grows by currents of vacancies from the area in $r < R - w_v/2$ and that in $r > R + w_v/2$. The growth rate of w_v at $r = R \pm w_v/2$ denoted by $\mathrm{d}w_v^{(\pm)}/\mathrm{d}t$ is described by the current at $r = R \pm w_v/2$ along $\mp\hat{\boldsymbol{r}}$, where $\hat{\boldsymbol{r}}$ is unit radial vector. Thus, $\mathrm{d}w_v^{(\pm)}/\mathrm{d}t$ is obtaind from eq. (5.5),

$$\begin{aligned} \frac{\mathrm{d}w_v^{(\pm)}}{\mathrm{d}t} &= \mp\frac{\partial}{\partial r}\{\frac{1}{2}B\psi^2(\boldsymbol{r}, t)\}|_{r=R\pm w_v/2} \\ &= \frac{B\psi_0^2}{w}\frac{\sinh(\frac{w_v}{2w})}{\cosh^3(\frac{w_v}{2w})}. \end{aligned} \tag{5.6}$$

From $\mathrm{d}w_v/\mathrm{d}t = \mathrm{d}w_v^{(+)}/\mathrm{d}t + \mathrm{d}w_v^{(-)}/\mathrm{d}t$, the equation of motion of w_v is obtained by

$$\frac{\mathrm{d}w_v}{\mathrm{d}t} = \frac{2B\psi_0^2}{w}\frac{\sinh(\frac{w_v}{2w})}{\cosh^3(\frac{w_v}{2w})}. \tag{5.7}$$

The growth rate of w_v takes the maximum value at $w_v = w\ln(2 + \sqrt{3})$ which is obtained from the maximum value of the right hand side of eq. (5.7). The formal solution

of eq. (5.7) is given by

$$\cosh^2(\frac{w_v}{2w}) + \ln\sinh(\frac{w_v}{2w}) = \frac{2B\psi_0^2}{w^2}t + c, \tag{5.8}$$

where c is a constant of integration. In the second stage, w_v is much smaller than w, so that the second term is dominant in the left hand side of the above equation by the expansion in power series of w_v/w. As a result, w_v satisfies the following euation:

$$w_v(t) = \exp\left\{\frac{B\psi_0^2}{w^2}t + c\right\}. \tag{5.9}$$

This growth law of w_v seems to indicate the dramatic rise of w_v in the time region between $2 \sim 5\times10^4$ and 10^5 steps in Fig. 6(b). On the other hand, the first term in the left hand side of eq. (5.8) gradually becomes dominant, as w_v becomes larger. Although the second term is not completely negligible even in the third stage, we neglect approximately the second term. Therefore, the growth law of w_v is given by

$$w_v(t) = w\ln\left\{\frac{8B\psi_0^2}{w^2}t + c\right\}. \tag{5.10}$$

This growth law is found in the time region after 10^5 steps in Fig. 6(b) for $B = 0.1$ and 0.2.

Next, we consider the growth law of R. The value of v around the interface in the vacancy-cluster is assumed constant as can be seen in Figs. 3(a) and 3(b), that is, the translational invariance of the interface is satisfied in the vacancy-cluster. Thus, an infinitegimal motion of the interface is approximately described by the same method as was developed by Kawasaki *et al.*[19,20] They formulated the method to derive the equation of motion of topological deffects from the phenomenological dynamical equation of the order parameter field. The growth law of R is analyzed by the method. The equation (5.3) is reduced to the following equation:

$$\int \mathrm{d}\boldsymbol{r}' G(\boldsymbol{r},\boldsymbol{r}')\frac{\partial\psi(\boldsymbol{r}')}{\partial t} = v(\boldsymbol{r})f(\psi(\boldsymbol{r})) - \int \mathrm{d}\boldsymbol{r}' f(\psi(\boldsymbol{r}'))\boldsymbol{\nabla}' v(\boldsymbol{r}')\cdot\boldsymbol{\nabla}' G(\boldsymbol{r},\boldsymbol{r}') + \phi(\boldsymbol{r}), \tag{5.11}$$

where $G(\boldsymbol{r},\boldsymbol{r}')$ is the Green function of the Poisson equation defined by $-\nabla^2 G(\boldsymbol{r},\boldsymbol{r}') = \delta(\boldsymbol{r}-\boldsymbol{r}')$. ϕ is an arbitrary function that satisfies $\nabla^2\phi = 0$. Integrating the above equation multiplied by $M'(r) = \psi_0\mathrm{sech}^2\{(r-R)/w\}$ over $\boldsymbol{r}$ gives

$$\int \mathrm{d}\boldsymbol{r}\int \mathrm{d}\boldsymbol{r}' M'(r)G(\boldsymbol{r},\boldsymbol{r}')\frac{\partial\psi(\boldsymbol{r}')}{\partial t} = \int \mathrm{d}\boldsymbol{r} M'(r)v(\boldsymbol{r})f(\psi(\boldsymbol{r})) - \int \mathrm{d}\boldsymbol{r}\int \mathrm{d}\boldsymbol{r}' M'(r)f(\psi(\boldsymbol{r}'))\boldsymbol{\nabla}' v(\boldsymbol{r}')\cdot\boldsymbol{\nabla}' G(\boldsymbol{r},\boldsymbol{r}') + \phi_0, \tag{5.12}$$

where $\phi_0 = \int \mathrm{d}\boldsymbol{r} M'(r)\phi(\boldsymbol{r})$. Taking into account of the assumpsion $R \gg w > w_v$ in the second stage, we evaluate terms in eq. (5.12) by a power series expansion of both w_v/w and w_v/R. As a result, the equation of motion of R is described by

$$\frac{\mathrm{d}R}{\mathrm{d}t}R^2\ln R = -\frac{\delta\sigma_0}{8w} - \frac{1-\delta}{8w^2}w_v + \phi_0 + O(\frac{w_v^3}{w^3}, \frac{w_v}{R}), \tag{5.13}$$

where $\sigma_0 = \frac{1}{w}\int \mathrm{d}r(\partial\psi(r)/\partial r)^2$ is a constant proportional to the interfacial energy per unit interfacial length. ϕ_0 is the term due to the conservation law which is expected the function with the complicated argument of time. Hereafter, we neglect ϕ_0, that is, the order parameter is supplied without the restriction of the conservation law. This is consistent with the assumption of the independence of δ on time. Substituting the approximate solution of w_v in the second stage, eq. (5.9), into the above equation, the formal solution of R is obtained.

$$\frac{1}{3}R^3(\ln R - \frac{1}{3}) = -\frac{\delta\sigma_0}{8w}t - \frac{1-\delta}{64\psi_0^2}\exp\{\frac{8\psi_0^2}{w^2}t + c\} + c', \tag{5.14}$$

where c' is a constant of integration. Since $\ln R$ in the left hand side of the eqation gives a correction, the growth law of R in the second stage is described as

$$R(t) \propto [c' - \frac{9\delta\sigma_0}{8w}t - \frac{9(1-\delta)}{64\psi_0^2}(\exp\{\frac{8\psi_0^2}{w^2}t + c\} - 1)]^{1/3}. \tag{5.15}$$

This equation is satisfied in the case for $w > w_v = \exp\{\frac{8\psi_0^2}{w^2}t + c\}$. The exponential term in eq. (5.15) seems to cause the rapid growth of the characteristic length in the early time stage, for example the time region between 10^4 and 10^5 for $v_0 = 0.001$ in Fig. 5(a). Here, we have to notice that R always decreses with time because of the interfacial tension. Therefore, we have to regard that only the qualitative time dependence of R corresponds that of the characteristic length. In the third stage, evaluating eq. (5.12) by a power series expansion of both $\exp\{-w_v/w\}$ and w_v/R, the equation of motion of R is given by

$$\frac{\mathrm{d}R}{\mathrm{d}t}R^2\ln R = -\frac{\delta\sigma_0}{8w} - \frac{(1-\delta)(1-3Bw^2/2)}{6w} - \frac{(1-\delta)Bw^2}{2w}\frac{w_v}{w}\mathrm{e}^{-w_v/w} + O(\mathrm{e}^{-w_v/w}, \frac{w_v}{R}). \tag{5.16}$$

If $Bw^2 \ll 1$, terms proportional to B in the right hand side of the above equation is negligible. Then, R satisfies the following equation:

$$R(t) = \left\{c' - [\frac{\delta\sigma_0}{8w} - \frac{(1-\delta)}{6w}]t\right\}^{1/3}. \tag{5.17}$$

Therefore, for small B, the characteristic length is expected to satisfy the power law of time with its exponent 1/3. This result is qualitatively the same as our numerical results in Fig. 5(a), although the exponent value is a little different. Moreover, the power law with its exponent 1/3 is predicted by Franzl-Penrose[11,12] and Puri-Sharma.[13,14] On the other hand, for large B, we cannot neglect two terms proportional to B in eq. (5.16). Then, substituting the approximate solution of w_v, eq. (5.10), into eq. (5.16), we obtain

$$R(t) = \Big\{c' - [\frac{\delta\sigma_0}{8w} - \frac{(1-\delta)(1-3Bw^2/2)}{6w}]t - \frac{(1-\delta)Bw^3}{16\psi_0^2}[\ln(\frac{8\psi_0^2}{w^2}t + c)]^2\Big\}^{1/3}. \quad (5.18)$$

Especially, if $B \simeq (3\delta\sigma_0 + 4(1-\delta))/6w^2$, the prefactor of the linear term of t in the above equation vanishes. Then, R obeys $[c' - b\ln(\frac{8\psi_0^2}{w^2}t + c)]^{2/3}$, where $b = (1-\delta)[3\delta\sigma_0 + 4(1-\delta)]/96$. Our numerical results in the third stage is qualitatively consistent with this growth law as in Fig. 5(b). Since the logarithmic function of time is introduced by the growth law of w_v, the growth law of the characteristic length for large B is found to relate with the growth law of w_v. The slowing down of the characteristic length is found in the late time stage in Fig. 5(b). We suppose that the slowing down is due to the lack of vacancies in stable domains. Consequently, it seems that the slowing down cannot be explained in our analytical approach, because the conservation law of the vacancy is not satisfied in our approach.

§6. Summary and Discussion

We formulate phenomenological dynamical equations for the vacancy-mediated phase separation from a mean-field free energy and perform the numerical simulation of the model. We also analytically interprete our numerical results. Summary and discussion of our results are as follows. (i) The scaling property of the scattering function is satisfied. The functional form of the scaling function depends on B. Moreover, the functional form in the case of the vacancy-mediated phase separation are different from that obtained by the CH equation. Vacancies cause the interfacial roughness because of the aggregation into the interfacial area. This causes differences among functional forms of the scaling function. (ii) Qualitative differences between the growth law of the characteristic length for $B = 0.1$ and that for $B = 0.4$ are found. Since currents of vacancies are proportional to B, dynamical properties of the vacancy-mediated phase separation depends on B. The characteristic length obeys the power law of time for small B. In the time region of our simulation, the exponent of the power law takes the value between 0.24 and 0.34. The exponent value may approach to the value 1/3 by longer time simulation. The characteristic length obeys the logarithmic function of time for large B and slows down in the late time stage in our simulation. Analytical approaches show the relation between the logarithmic growth law of the characteristic length and the growth law of the width of the vacancy-cluster and indicate that the characteristic length for small B obeys the power law of time with its exponent 1/3, while the characteristic length for large B obeys the power law of the logarithmic function of time with the exponent 2/3. (iii) The width of the interfacial area increases with the growth of the vacancy-cluster in the interfacial area. As a result, for large v_0, the width of the interfacial area grows with the logarithmic function of time in the late time region when the width of the vacancy-cluster approaches to that of the interfacial area. On the other hand, for small v_0, the width of the interfacial area takes almost constant value even in the late time region, because the width of the interfacial area is larger than that of the vacancy cluster. (iv) The width of the vacancy-cluster grows with the logarithmic function of time in the late time region. This growth law is also analytically obtained from our model. The dynamical properties of the vacancy-mediated phase separation for large B have a significant difference from those of the phase separation by the exchange mechanics. Yaldram and Binder[9,10] indicated that changing vacancy concentration meant only the change of time scale. In our model, changing B may be the change of time scale, although other quantities may also have to be scaled by B simultaneously. This is a possible future problem.

Acknowledgements

I would like to thank Dr. S. Puri for suggesting this problem and valuable discussions.

1) G. E. Murch: *Materials Science and Technology Vol. 5, Phase Transformations in Materials*, ed. R. W. Cahn, P. Haasen and E. J. Kramer (VCH, Weinheim, 1991) p. 75.
2) K. Kawasaki: *Phase Transitions and Critical Phenomena* Vol. 2, ed. C. Domb and M. S. Green (Academic Press, New York, 1972) p. 443.
3) J. W. Cahn and J. I. Hilliard: J. Chem. Phys. **28** (1958) 258.
4) J. D. Gunton, M. S. Miguel and P. S. Sahni: *Phase Transitions and Critical Phenomena* Vol. 8, ed. C. Domb and J. L. Lebowitz (Academic Press, London, 1983).
5) S. Komura: Phase Transit. **12** (1988) 3.
6) R. Wagner and R. Kampmann: *Materials Science and Technology Vol. 5, Phase Transformations in Materials* ed. R. W. Cahn, P. Haasen and E. J. Kramer (VCH, Weinheim, 1991) p. 213.
7) K. Binder: *Materials Science and Technology Vol. 5, Phase Transformations in Materials*, ed. R. W. Cahn, P. Haasen and E. J. Kramer (VCH, Weinheim, 1991) p. 405.
8) A. J. Bray: Adv. Phys. **43** (1994) 357.
9) K. Yaldram and K. Binder: Z. Phys. B **24** (1991) 405.
10) K. Yaldram and K. Binder: Acta. Metall. Mater. **39** (1991) 404.
11) P. Fratzl and O. Penrose: Phys. Rev. B **50** (1994) 3477.
12) P. Fratzl and O. Penrose: Phys. Rev. B **55** (1997) R6101.
13) S. Puri: Phys. Rev. E **55** (1997) 1752.
14) S. Puri and R. Sharma: Phys. Rev. E **57** (1998) 1873.
15) P. Weiss: J. Phys. **6** (1907) 667.
16) T. M. Rogers, K. R. Elder and R. C. Desai: Phys. Rev. B **37** (1988) 9638.
17) T. M. Rogers and R. C. Desai: Phys. Rev. B **39** (1989) 11956.
18) I. M. Lifshits and V. V. Slyozov: Phys. Chem. Solids **19** (1961) 35.
19) K. Kawasaki: Ann. Phys. **154** (1984) 319.
20) S. Ohta, T. Ohta and K. Kawasaki: Physica A **128** (1984) 1.